Available online at www.sciencedirect.com
SCIENCE DIRECT
Journal of Sound and Vibration 296 (2006) 518–538
JOURNAL OF SOUND AND VIBRATION
www.elsevier.com/locate/jsvi

A new temporal method for the identification of source directions in a reverberant hall

C. Noël[a], V. Planeau[a], D. Habault[b,*]

[a]Institut National de Recherche et de Sécurité, avenue de Bourgogne B.P. 27, 54501 Vandoeuvre, France
[b]CNRS-Laboratoire de Mécanique et d'Acoustique, 31 chemin Joseph Aiguier, 13402 Marseille Cedex 20, France

Received 9 September 2004; received in revised form 30 November 2005; accepted 15 December 2005
Available online 19 June 2006

Abstract

The study presented here is related to the reduction of noise in factory halls. The type of factory hall considered here has large dimensions and contain several industrial machines, running 24 h a day. A method is presented to determine the angular directions which provide the main contributions to the sound levels at any point in the hall. These directions correspond to the sources and their images on the walls and on the obstacles. The method is based on the use of cross-correlation functions of sound signals measured on a microphone array. It is adapted to the constraints of the problem (short measurement time, no possibility to stop the machines, small dimensions of the array, etc.). Experimental results are shown first for several test cases carried out in a semi-anechoic room and in a rectangular room, and, then, for the case of a surface-planing machine in a cluttered hall.

1. Introduction

The study presented here is concerned with noise-reduction problems that are commonly encountered in factory halls. These halls typically have large dimensions, reflecting walls, and they contain noisy engines or machines that run constantly, 24 h a day. In many practical applications of noise abatement in factory halls, the main point is not really to reduce the noise levels everywhere in the hall, but rather to protect some particular work places. As a consequence, what is needed is generally not a full acoustic treatment of the entire hall, but only a limitation of sound reflections on some surfaces in the hall. The reason is that the sound field, at any point, is a combination of the various contributions from all actual acoustic sources and from the reflections produced by the walls and obstacles present in the hall. Thus, to reduce the sound level at a given point in the hall, one first thing to do is to determine the main directions of incidence from which energy reaches this point. If these directions can be correctly identified, it is then possible to decide which machines and which parts of the hall should be treated. The treatment may consist in partly or totally enclosing a machine, in inserting acoustic screens between the source and the place to protect, in sticking absorbing materials on the corresponding wall, etc.

*Corresponding author. Tel.: +33 491 164 069; fax: +33 491 164 080.
E-mail address: habault@lma.cnrs-mrs.fr (D. Habault).

0022-460X/$ - see front matter © 2006 Elsevier Ltd. All rights reserved.
doi:10.1016/j.jsv.2005.12.056

In the present paper, a new method is described that allows one to determine the direction of incidence of a sound, produced by a set of fixed sources, at any point in a large-dimension hall with highly reflecting walls. The method is based on the measurements of the sound field by a microphone array, with the following assumptions:

- the dimensions of the array must be kept as small as possible, as well as the number of microphones,
- the time necessary to run a complete set of measures must be as short as possible,
- measurements should be possible while the machines are constantly in action,
- the method has to apply to correlated fields, such as those produced by a sound source and its images.

An extensive review of the literature on the existing methods for sound-incidence identification reveals that none can meet the requirements listed above.

Classical intensimetry techniques were first considered for this purpose, but it has been shown that they are efficient mainly in the near field of a source, or in rooms with rather absorbing walls [1,2]. For these reasons and because they are not selective enough, they were discarded.

Another group of theoretical methods, called matched-field methods, has also been developed, based on an analysis of the sound in the frequency domain, to identify acoustic-wave directions. Most of them use the cross-spectral densities of the sound signals measured with the help of an array. Among the most popular are the Bartlett estimator, Minimum Variance Distortionless Filter (MVDF) and MUltiple SIgnal Classification (MUSIC). They were first developed for periodic signals [3–8]. Bartlett estimator is not adapted to the applications considered here because the number of microphones required for the measurements is too large [3]. MVDF and MUSIC are not efficient to separate out correlated sound fields [9–11]. Later on, these methods have been extended to the case of broad-band sources, using two different approaches based respectively on incoherent and coherent focusing [12,13]. Both approaches are based on a global cross-spectral density matrix which is defined as the mean value of the cross-spectral density matrices obtained at all frequencies [14,15]. For incoherent focusing, this mean value is calculated as a geometrical or an arithmetical mean value. For coherent focusing, the matrices are first multiplied by the so-called focusing operators [16,17]. With this last approach, it is possible to determine the position of correlated sources [18,19]. However, the number of sources must be smaller than the number of microphones. This condition cannot be met in the case of a factory hall because of the number of machines and of the reflections on the walls.

Identification methods have also been developed in the time domain. One group is based on the measurement of impulse responses on an array. They are used to determine the positions of the sources and their amplitudes or to analyze the directions and the spatial variations of a reverberant sound field [20–23]. This kind of technique is obviously not relevant in our case because, as mentioned above, industrial machines cannot always be switched off and on again whenever needed for measurements. Another group is based on the use of the time delays measured between all the pairs of microphones of an array [24,25].

The method presented here, called ISIT, belongs to this last group. The name ISIT comes from the French expression for ''identification of sources by a cross-correlation technique''. It is an optimization method based on the use of the cross-correlation functions of the signals measured on an array. The unknowns to be determined represent the angular flow of energy received from each direction of space. They are obtained by minimizing the difference between theoretical and measured values of a time integral of the cross-correlation functions. The main directions that contribute to the sound pressure on the array are deduced from the values of these unknowns.

Section 2 presents the theoretical development and the assumptions used to construct the method. This leads to the minimization of an overdetermined system with constraints. The numerical aspects related to the computation of the matrix of the system are studied in Section 3. Section 4 presents the criteria used to design the array best fitted to the method. Section 5 examines how the method applies in practical cases where the theoretical assumptions not all satisfied. Section 6 describes some experimental tests carried out for two simple configurations: one source and its images in a semi-anechoic room first, and then one and two sources in an reverberant rectangular hall. Section 7 presents the results in a more realistic case of a surface-planing machine in a cluttered hall. Section 8 presents the conclusion of the study.

2. Description of the method

The method consists in a comparison between calculated and measured values of time integrals of cross-correlation functions. These time integrals are expressed as functions of the angular energy flow.

The first step is to obtain an expression of a cross-correlation function between two receivers, based on the following assumptions:

- the receivers are in the far field of the sources,
- the sound field is approximated by a large number of plane waves,
- the sound field is homogeneous and anisotropic. This means that the cross-correlation function between two points P and M only depends on the distance between these two points and on the angle between the vector **PM** and the direction of propagation [26],
- the plane waves are uncorrelated and have "white noise" spectra.

The influence of these assumptions in the practical applications of the method is examined in detail in Section 5.

The sound pressure is measured at N points corresponding to the N microphones of an array. Let $x_n(t)$ and $x_m(t)$, $n = 1, \ldots, N$ and $m = 1, \ldots, N$, be the sound signals measured at two points M_n and M_m. If d_{nm} denotes the distance between M_n and M_m, the corresponding vector $\mathbf{r}_{nm}$ is given by

$$\mathbf{r}_{nm} = d_{nm}[\sin\theta_c \cos\phi_c, \sin\theta_c \sin\phi_c, \cos\theta_c], \tag{1}$$

where the angles are defined in Fig. 1.

The expression of the cross-correlation function $C_{x_n,x_m}(\tau)$ between the signals $x_n(t)$ and $x_m(t)$ is deduced from equations similar to the ones presented in Refs. [26–28].

The pressure signals are assumed to be random and stationary in time. In the case of a single plane wave characterized by two angles ϕ and θ or equivalently by the vector $\mathbf{n}(\phi, \theta)$:

$$\mathbf{n}(\phi, \theta) = [\cos\phi \sin\theta, \sin\phi \sin\theta, \cos\theta] \tag{2}$$

the sound pressure measured at a receiver M can be written:

$$p(M; \phi, \theta, v) = A(\phi, \theta, v) \exp\left(-2i\pi v \frac{\mathbf{n}(\phi, \theta).\mathbf{OM}}{c}\right), \tag{3}$$

where c is the sound velocity in the fluid and v the frequency. **OM** is the vector between the space origin O and the receiver point. The operator "." represents the scalar product of the vectors **n** and **OM**.

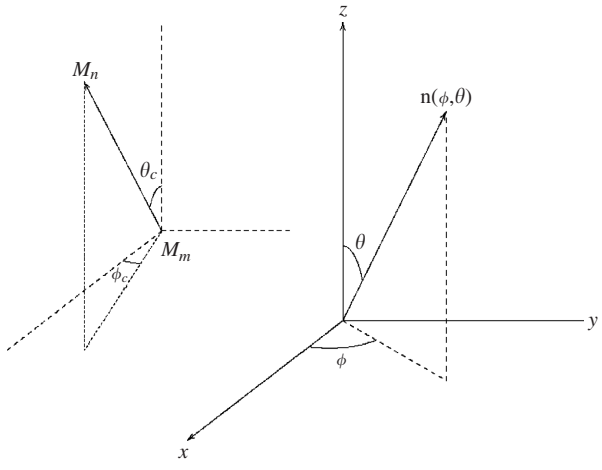

Fig. 1. Notations.

If the sound field is composed of an infinite number of plane waves, coming from all possible directions, the sound field can be written as

$$P(M;v) = \int_{\Omega} p(M;\phi,\theta,v)\sin\theta\,\mathrm{d}\theta\,\mathrm{d}\phi, \tag{4}$$

where $\Omega = \{0 \leqslant \phi \leqslant 2\pi,\ 0 \leqslant \theta \leqslant \pi\}$ is the space of the angles of incidence (ϕ,θ).

If all these plane waves are not correlated, the cross-spectral density between two receivers M_n and M_m is equal to

$$\begin{aligned} S_{x_n,x_m}(v) &= E(P(M_n,v)P^*(M_m,v)) \\ &= \int_{\Omega} E(|A(\phi,\theta,v)|^2)\exp\left(-2\mathrm{i}\pi v\frac{\mathbf{n}(\phi,\theta).\mathbf{r}_{nm}}{c}\right)\sin\theta\,\mathrm{d}\theta\,\mathrm{d}\phi. \end{aligned} \tag{5}$$

Furthermore if the expression $E(|A(\phi,\theta,v)|^2)$ does not depend on frequency—which is the case of "white noise" spectra—it can be written as

$$E(|A(\phi,\theta,v)|^2) = \alpha(\phi,\theta). \tag{6}$$

$\alpha(\phi,\theta)$ has the dimensions of $(\text{pressure})^2(\text{frequency})^{-1}(\text{surface})^{-1}$. It corresponds to an angular energy flow [26].

The cross-correlation function is finally obtained by using an inverse Fourier transform

$$C_{x_n,x_m}(\tau) = \int_{\Omega} \alpha(\phi,\theta)\delta\left(\tau - \frac{\mathbf{n}(\phi,\theta).\mathbf{r}_{nm}}{c}\right)\sin\theta\,\mathrm{d}\theta\,\mathrm{d}\phi, \tag{7}$$

where τ is the time delay and δ stands for the Dirac distribution.

Next the space Ω is divided into K cells Ω_l, $l = 1,\ldots,K$, of constant width $(\Delta\phi,\Delta\theta)$ as shown in Fig. 2. They are supposed to be small enough so that the energy flow $\alpha(\phi,\theta)$ may be approximated by a constant α_l on each Ω_l.

This leads to

$$C_{x_n,x_m}(\tau) = \sum_{l=1}^{l=K} \alpha_l \int_{\Omega_l} \delta\left(\tau - \frac{\mathbf{n}(\phi_l,\theta_l).\mathbf{r}_{nm}}{c}\right)\sin\theta_l\,\mathrm{d}\theta_l\,\mathrm{d}\phi_l. \tag{8}$$

Let $\Delta\Omega_l$ denote the integral on the cell Ω_l: $\Delta\Omega_l = \int_{\Omega_l}\sin\theta_l\,\mathrm{d}\theta_l\,\mathrm{d}\phi_l$. The energy term E_l corresponding to a cell Ω_l is defined by

$$E_l = \alpha_l\Delta\Omega_l \tag{9}$$

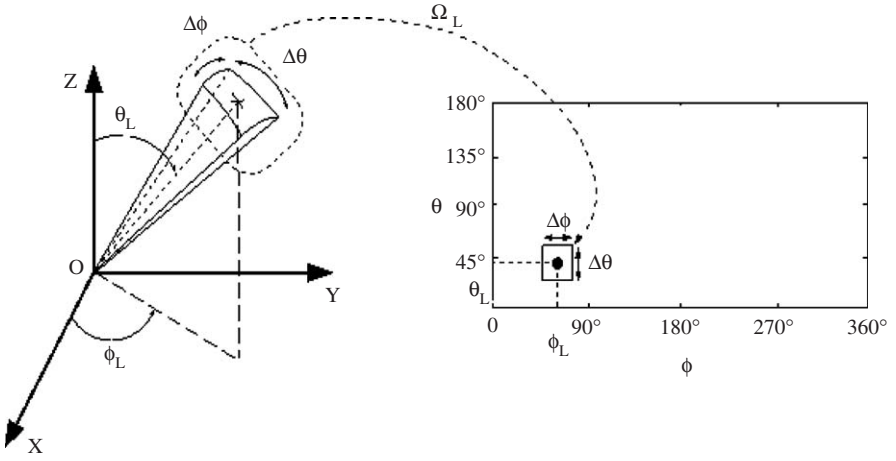

Fig. 2. Mesh of space Ω.

and C_{x_n,x_m} is written

$$C_{x_n,x_m}(\tau) = \sum_{l=1}^{l=K} E_l \frac{\int_{\Omega_l} \delta\left(\tau - \dfrac{\mathbf{n}(\phi_l,\theta_l).\mathbf{r}_{nm}}{c}\right) \sin\theta_l \,\mathrm{d}\theta_l \,\mathrm{d}\phi_l}{\Delta\Omega_l}. \tag{10}$$

The coefficients $E_l, l = 1,\ldots,K$ are the unknowns of the problem. If there is no energy coming from directions corresponding to a cell Ω_l, the value of E_l is equal to zero. The largest values of E_l provide the main directions that contribute to the sound level at the position of the array.

Let us remark that, in practical applications, several waves with different amplitudes can contribute to the same integral on one cell Ω_l. The method will take their contributions into account as the contribution of one and only one wave. This means that the size of the mesh must be chosen as small as possible. The applications presented in the last sections of this paper provide examples of results in this kind of situations.

The coefficients E_l are obtained by minimizing the difference between theoretical and measured values of the time integral of the cross-correlation functions.

Before integrating, it must be remarked that, in the case of plane waves coming only from the direction defined by (ϕ_i,θ_i) corresponding to a cell Ω_i, $C_{x_n,x_m}(\tau)$ is zero for τ outside the interval $I^i_{nm} = [\tau^i_{\min}(n,m); \tau^i_{\max}(n,m)]$ with:

$$\begin{cases} \tau^i_{\min}(n,m) = \min\limits_{(\phi_i,\theta_i)\in\Omega_i} \dfrac{\mathbf{n}(\phi_i,\theta_i).\mathbf{r}_{nm}}{c}, \\ \tau^i_{\max}(n,m) = \max\limits_{(\phi_i,\theta_i)\in\Omega_i} \dfrac{\mathbf{n}(\phi_i,\theta_i).\mathbf{r}_{nm}}{c} \end{cases} \tag{11}$$

because of the Dirac function in formula (10). The integration of the cross-correlation function on this interval I^i_{nm} and the inversion of the integral and the sum give the following equation:

$$C^i(n,m) = \sum_{l=1}^{l=K} E_l \beta^i_l(n,m) \tag{12}$$

with

$$C^i(n,m) = \int_{I^i_{nm}} C_{x_n,x_m}(\tau_i)\,\mathrm{d}\tau_i, \tag{13}$$

$$\beta^i_l(n,m) = \frac{\int_{I^i_{nm}} \int_{\Omega_l} \delta\left(\tau_i - \dfrac{\mathbf{n}(\phi_l,\theta_l).\mathbf{r}_{nm}}{c}\right) \sin\theta_l \,\mathrm{d}\theta_l \,\mathrm{d}\phi_l \,\mathrm{d}\tau_i}{\Delta\Omega_l}. \tag{14}$$

Eq. (12) must be satisfied for every $i = 1,\ldots,K$. The coefficients E_l can be obtained as the solutions of the linear system:

$$\mathbf{C}(n,m) = \mathbf{B}(n,m)\mathbf{E} \tag{15}$$

with

$$\mathbf{C}(n,m) = (C^i(n,m)),\ \ i = 1,\ldots,K, \quad \mathbf{E} = (E_l),\ \ l = 1,\ldots,K \tag{16}$$

and

$$\mathbf{B}(n,m) = (\beta^i_l(n,m)), \quad i = 1,\ldots,K \text{ and } l = 1,\ldots,K. \tag{17}$$

This system is of order K. However, Eq. (15) must be satisfied for all pairs of microphones (M_n, M_m) with $n \neq m$. This means that the coefficients E_l are solutions of a linear system of $N_c K$ equations, where N_c is the number of pairs of microphones. This linear system is written

$$\mathbf{B}_g\mathbf{E} = \mathbf{C}_g, \tag{18}$$

where the global vector $\mathbf{C}_g$ and the global matrix $\mathbf{B}_g$ are built from all vectors $\mathbf{C}(\mathbf{n},\mathbf{m})$ and all matrices $\mathbf{B}(\mathbf{n},\mathbf{m})$ respectively:

$$\mathbf{C}_g = \begin{bmatrix} \mathbf{C}(1,2) \\ \vdots \\ \mathbf{C}(j,k) \\ \vdots \\ \mathbf{C}(N-1,N) \end{bmatrix} \quad \text{and} \quad \mathbf{B}_g = \begin{bmatrix} \mathbf{B}(1,2) \\ \vdots \\ \mathbf{B}(j,k) \\ \vdots \\ \mathbf{B}(N-1,N) \end{bmatrix}. \tag{19}$$

$\mathbf{C}_g$ is a vector of order N_cK. $\mathbf{B}_g$ is a rectangular matrix of order $N_cK \times K$. The unknown vector $\mathbf{E}$ is the solution of the overdetermined system (18). It is obtained by solving a least-squares minimization problem with constraints:

$$\min_{\mathbf{E}} \|\mathbf{B}_g\mathbf{E} - \mathbf{C}_g\|^2 \quad \text{with} \quad E_l \geqslant 0,\ l = 1,\ldots,K. \tag{20}$$

This problem is solved by the non-negative least-squares algorithm (NNLS) described in Ref. [29].

3. Computation of the matrix B

The computation of the global matrix $\mathbf{B}_g$ is the main step of the numerical procedure. Two aspects are presented here, the computation of the coefficients $\beta_l^i(n,m)$ of the matrix and the procedure chosen to construct the global matrix.

3.1. Computation of the coefficients of the matrix $\mathbf{B}(n,m)$

As mentioned before, the global matrix $\mathbf{B}_g$ contains N_cK^2 coefficients. In the examples presented in this article, the angular width of the cells $\Delta\phi$ and $\Delta\theta$ are chosen equal to 10°. This leads to a number of cells equal to $36 \times 18 = 648$. Also in the examples, the number N_c of pairs of microphones is equal to 105. This means that the order of magnitude of N_cK^2 is around 41×10^6. Therefore it is essential to develop a method to drastically reduce the computation time for the $\beta_l^i(n,m)$ terms.

Each coefficient $\beta_l^i(n,m)$ is expressed in Eq. (14) as an integral over time τ and over angles ϕ and θ. This integral must be calculated with a very small time step because it includes a Dirac distribution. To reduce computation time, several methods were developed and compared. The best results, for the criterion of computation time versus accuracy, are obtained by using infinite series of Legendre polynomials. The main steps of the method are presented here and the details are given in Appendix A.

Let us start with the cross-spectral function $S_{x_n,x_m}(v)$ defined in formula (5):

$$S_{x_n,x_m}(v) = \int_\Omega \alpha(\phi,\theta) \exp\left(-2\mathrm{i}\pi v \frac{\mathbf{n}(\phi,\theta).\mathbf{r}_{nm}}{c}\right) \sin\theta \,\mathrm{d}\theta \,\mathrm{d}\phi. \tag{21}$$

In this expression, the exponential function is replaced by its series in spherical harmonics. After some analytical integrations, $S_{x_n,x_m}(v)$ is obtained as

$$S_{x_n,x_m}(v) = \sum_{l=1}^{l=K} \frac{E_l}{\Delta\Omega_l} \sum_{p=0}^{p=+\infty} (-i)^p \gamma_p^l j_p(kd_{nm}), \tag{22}$$

where j_p is the spherical Bessel function of order p and of the first kind. The expression of the γ_p^l coefficients is given in Eq. (A.8) of Appendix A. Then, the cross-correlation function is expressed as the inverse Fourier transform of $S_{x_n,x_m}(v)$. Again, some integrations can be done analytically and finally the integration of C_{x_n,x_m} on the interval I_{nm}^i yields

$$C^i(n,m) = \sum_{l=1}^{l=K} E_l \frac{1}{\Delta\Omega_l} \sum_{p=0}^{p=+\infty} \frac{(-1)^p}{2} \gamma_p^l \int_{A_{nm}^i} P_p(\tau)\,\mathrm{d}\tau, \tag{23}$$

where P_p is the Legendre polynomial of degree p and A^i_{nm} is the interval defined by

$$A^i_{nm} = \left[-\frac{c}{d_{nm}} \tau^i_{\max}(n,m); -\frac{c}{d_{nm}} \tau^i_{\min}(n,m) \right]. \tag{24}$$

Finally, from Eqs. (12) and (23), and for $i = 1, \ldots, K$ and $l = 1, \ldots, K$:

$$\beta^i_l(n,m) = \frac{1}{\Delta\Omega_l} \sum_{p=0}^{p=+\infty} \frac{(-1)^p}{2} \gamma^l_p \int_{A^i_{nm}} P_p(\tau)\, \mathrm{d}\tau. \tag{25}$$

This formula is easier to compute than formula (14). It includes an infinite series and a simple integral. In our examples, the series converges rapidly, it is approximated with no more than 50 terms. Formula (25) leads to shorter computation time than formula (14).

3.2. Reduction of the order of the linear system

To obtain accurate results, the rank of the global matrix $\mathbf{B}_g$ must be as close as possible to the order of the matrix. This means that $\mathbf{B}_g$ must be well conditioned. This matrix is built from the elementary square matrices $\mathbf{B}(n,m)$ defined by Eq. (17). The values of the coefficients and therefore the rank of the matrix closely depend on the positions of the microphones. In particular, it is easily seen that two elementary matrices $\mathbf{B}(n,m)$ and $\mathbf{B}(p,q)$ provide the same information if the four points M_n, M_m, M_p, M_q are such that the vectors $\mathbf{r}_{nm}$ and $\mathbf{r}_{pq}$ are collinear, that is, if $\mathbf{r}_{nm} = a\mathbf{r}_{pq}$ where a is a constant.

To obtain the highest possible value for the rank of $\mathbf{B}_g$, it is necessary, first to carefully select the positions of the pairs of sensors in order to maximize the ranks of the elementary matrices, and then to use a large number of elementary matrices $\mathbf{B}(n,m)$. This implies that the global matrix is quite big. Therefore, a singular value decomposition (SVD) method is used to reduce the order of the global linear system. This leads to a reduced matrix $\mathbf{B}_r$ of order K and a vector $\mathbf{C}_r$ of order K such that the linear system in Eq. (18) is replaced by

$$\mathbf{B}_r \mathbf{E} = \mathbf{C}_r, \tag{26}$$

where the singular values of $\mathbf{B}_r$ are equal to the K largest singular values of the matrix $\mathbf{B}_g$. The SVD method is not used for the global matrix itself because of its large size. To avoid having to handle with too big a matrix and in order to minimize the round-off errors, the SVD method is applied to submatrices of $\mathbf{B}_g$ in an iterative way.

The computation of the global matrix is the part of the method that is the most time-consuming. This step may take several hours (between 5 and 10) on a classical PC (450 MHz, 256 Mb) but the matrix is computed only once because it depends only on the geometry of the array. In contrast, the minimization step runs very fast and the coefficients E_l are obtained within less than 5 min for each case.

4. Choice of an array

As said previously, for practical reasons, it was decided to keep the number of microphones and the dimensions of the array as small as possible. The maximum number of microphones was restricted to 15 and the maximum length of the array to 0.5 m.

Several criteria have been considered to define the shape of the array and to determine the position of each microphone. The two main criteria, which are detailed below, are strongly related to the ISIT method and its numerical procedure.

The first one is related to the computation of the coefficients $C^i(n,m)$. They are defined as integrals over intervals I^i_{nm} of the cross-correlation function $C_{x_n,x_m}(\tau)$. Each function $C_{x_n,x_m}(\tau)$ is measured with a sampling frequency F_e. Each interval I^i_{nm} depends on several parameters, in particular the angular widths $\Delta\phi$ and $\Delta\theta$, and the distance d_{nm}. In order to compute accurate values of the integrals over I^i_{nm}, these parameters cannot be chosen independently. Here we have chosen a sampling frequency equal to 25.6 kHz and an angular width $\Delta\phi = \Delta\theta = 10^\circ$. Several numerical tests have been carried out. They show that the integrals are fairly

accurately computed if the distance d_{nm} is larger that 0.2 m. It was therefore decided to keep the distances between all pairs of microphones between 0.2 and 0.5 m.

The other aspect is related to the rank of the global matrix $\mathbf{B}_g$. As seen in Section 3.2, it is necessary to keep the number of collinear vectors as small as possible. Here, the positions of the microphones have also been chosen in such a way that the logarithm of the ratio between the highest and the lowest singular values of the global matrix $\mathbf{B}_g$ is smaller than 30 dB. This ratio is called the condition number of the matrix. Obviously, it is not possible to relate it to the positions of the microphones in a straightforward way: For a given set of positions, the value of the ratio cannot be a priori assessed. This limiting value of 30 dB has been chosen after several series of tests and according to the values of signal-to-noise ratio in our practical applications.

Several microphone arrays have been numerically tested, in particular:

- a classical cross-shaped array with 13 microphones,
- a pyramid-shaped array made of equilateral pyramids, with 11 microphones (see Fig. 3). The length of each side is equal to 0.3 m and there are 64 non-collinear vectors,
- a spherical array with 15 microphones and a radius equal to 0.25 m (see Figs. 4 and 5). The 15 microphones are located on three parallel circles in such a way that the number of collinear vectors is kept to a minimum. In this case, 75 vectors are non-collinear. The distances between the microphones go from 0.21 to 0.5 m.

The three curves in Fig. 6 represent the values of the logarithm of the condition number obtained for these three arrays. They are drawn as a function of the number of cells chosen for the angular mesh. The maximum value on the horizontal scale (648 cells) corresponds to an angular step of 10° in both directions ϕ and θ. The spherical array has finally been chosen because it provides the lowest value for the condition number of matrix $\mathbf{B}_g$ and corresponds to a simple geometry. Let us remark that the choice of spherical arrays is also usual in some beamforming techniques or decomposition techniques for diffuse fields (see Ref. [30] and references within for example).

5. Discussion on the assumptions

In Section 2, several assumptions are made on the signals (white-noise spectra, uncorrelated plane waves). These assumptions are not always satisfied in practical applications. The aim of this section is to examine the

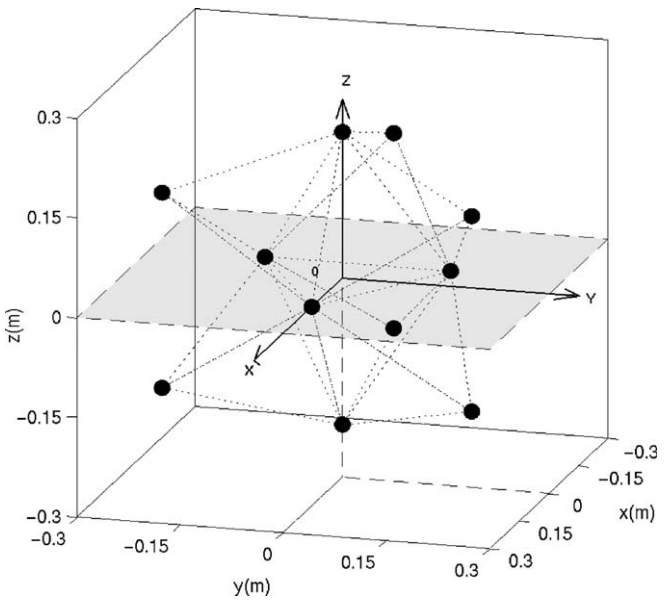

Fig. 3. Pyramid-shaped array.

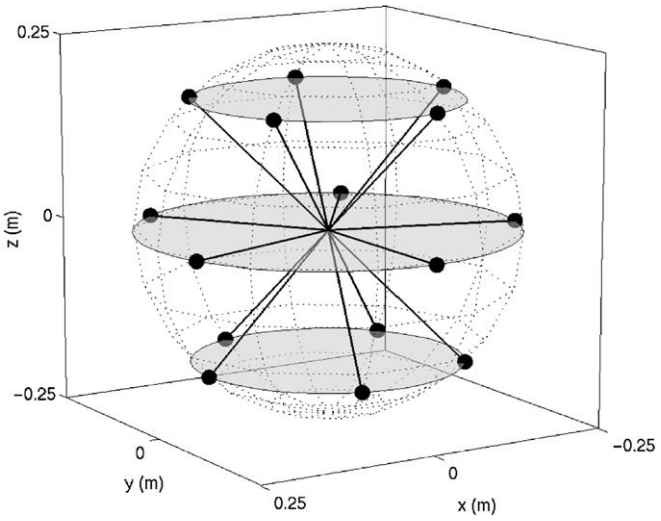

Fig. 4. Spherical array.

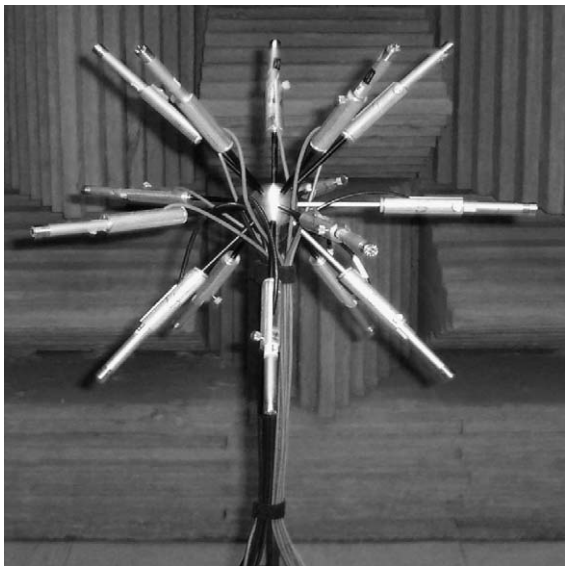

Fig. 5. View of the spherical array.

conditions for which the theoretical procedure may be applied or must be modified. The first hypothesis is that the array is situated in the far field of the sources to be localized. This is generally the case.

5.1. Sources with a broad-band spectrum different from a white noise

One of the assumptions is that the signals have a wide spectrum with constant power density (white noise type). This is not the case in practice. However, industrial machines are often broad-band sources and thus the cross-spectral densities obtained from the signals received at each microphone can be "whitened" by a classical technique, here a PHAse Transform is used [31]. This implies that the information on the phase of the spectra is preserved, but the amplitudes may be lost after this step. If the method is applied to identify one source and its images, because the spectra of the source and all the echoes have the same characteristics, they are processed similarly at the whitening stage. In this case, the respective amplitudes are not lost. If the method is

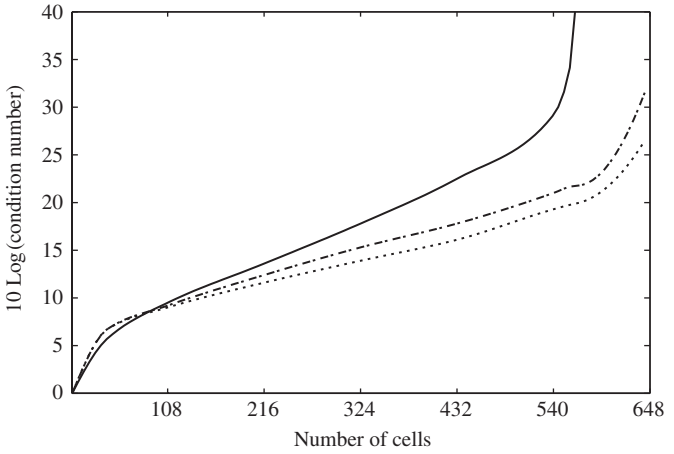

Fig. 6. 10*Logarithm of the condition number of matrix $\mathbf{B}_g$ as a function of the number of cells. Cross-shaped array (solid line); pyramid array (dashed line); spherical array (dotted line).

applied to two sources with different spectra, for example, a source A with a 0–5000 Hz spectrum and a source B with a 5000–10 000 Hz spectrum, the method will provide the correct directions but will not provide the respective amplitudes of the sources.

5.2. Sources with a narrow-band spectrum

If the emitted signals have a limited spectral bandwidth b_d, Eq. (2) becomes

$$E(|A(\phi,\theta,v)|^2) = \alpha(\phi,\theta)\Lambda(v), \tag{27}$$

where Λ is the function equal to 1 for v in the interval $[-b_d, +b_d]$ and 0 outside. The cross-correlation function becomes

$$C_{x_n,x_m}(\tau) = 2b_d \int_\Omega \alpha(\phi,\theta) \frac{\sin 2\pi b_d\left(\tau - \dfrac{\mathbf{n}(\phi,\theta).\mathbf{r}_{nm}}{c}\right)}{2\pi b_d\left(\tau - \dfrac{\mathbf{n}(\phi,\theta).\mathbf{r}_{nm}}{c}\right)} \sin\theta \,\mathrm{d}\theta \,\mathrm{d}\phi. \tag{28}$$

In this case, erroneous directions will appear. As an example, let us take the simple case of a single plane wave with a direction (ϕ,θ) corresponding to a time delay τ_0 between microphones M_n and M_m.

If this wave has a broad-band spectrum, $C_{x_n,x_m}(\tau) = \alpha(\phi,\theta)\delta(\tau-\tau_0)\sin\theta$. All coefficients $C^j(n,m)$ are equal to zero except those such that τ_0 belongs to $I^j_{n,m}$. Let us recall that the intervals $I^j_{n,m}$ may overlap. For a given pair (n,m), $C^j(n,m) \neq 0$ a priori means that cell Ω_j might correspond to the direction of the plane wave. Solving the minimization system (Eq. (20)) will provide the correct unique solution (ϕ,θ).

If the spectral bandwidth is equal to b_d, the cross-correlation reduces to

$$C_{x_n,x_m}(\tau) = \alpha(\phi,\theta)\frac{\sin 2\pi b_d(\tau-\tau_0)}{\pi(\tau-\tau_0)}\sin\theta. \tag{29}$$

Because of the shape of this function of τ, integration on some intervals $I^j_{n,m}$ which do not contain τ_0 will lead to non-zero coefficients $C^j(n,m)$. Fig. 7 shows an example of both cross-correlation functions obtained for $\tau_0 = 0.43$ ms as functions of time τ. The solid line represents the delta function. The dashed line represents the time function in Eq. (29) computed for $b_d = 2$ kHz. Both curves are normalized so that their maximum is equal to 1. For both functions, integration on interval Γ_b gives a non-zero value. Integration on interval Γ_a is zero for the delta function and non-zero for the other function. This will lead to erroneous solutions of the optimization problem. Obviously the error made depends on the relative values of the bandwidth and of the

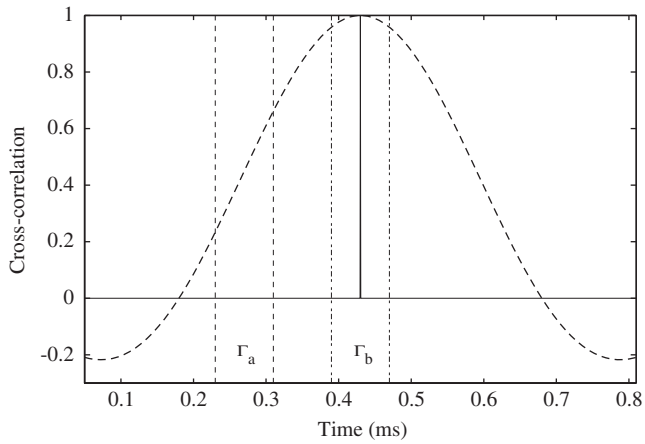

Fig. 7. Normalized cross-correlation functions versus time τ, for $\tau_0 = 0.43$ ms. Delta function (solid line); Eq. (29) for $b_d = 2$ kHz (dashed line). Γ_a and Γ_b represent two integration intervals.

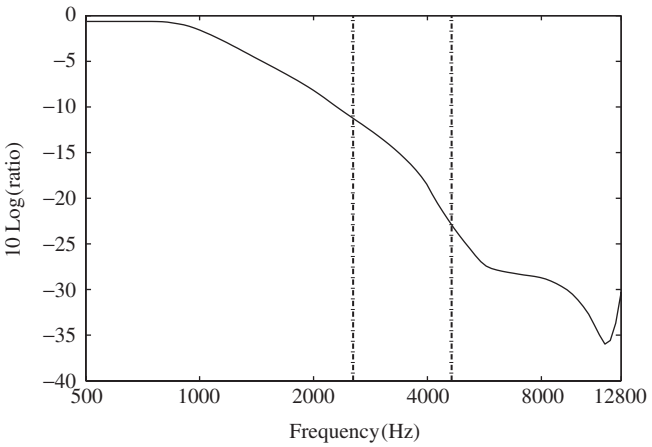

Fig. 8. 10*Logarithm of the ratio between the second and the first largest coefficients of the solution **E** as a function of the bandwidth of the signal emitted by the source.

width of the integration intervals. The integration intervals depend on the angular size of the mesh. This means that the bandwidth of the signals emitted by the sources must be taken into account to choose the angular size of the mesh.

In what follows, we present a numerical test that shows the influence of the signal bandwidth b_d on the solution **E** obtained for a given mesh. The angular width is 10° for ϕ and θ. The sound field is emitted by a single plane wave of direction (ϕ_0, θ_0). The ISIT method provides a solution **E**. Because there is only one source, all coefficients E_l should be equal to zero except one. Actually, as expected from the comments above, several coefficients have values different from zero. The largest coefficient does correspond to the exact direction (ϕ_0, θ_0). The curve in Fig. 8 represents the logarithm, multiplied by 10, of the ratio between the second and the first largest coefficients of vector **E**. The curve is drawn as a function of b_d, from 500 to 12 800 Hz. For each value of b_d, the value of the curve is the average of the values obtained over 20 tests corresponding to 20 different directions (ϕ_0, θ_0).

For b_d between 500 and 2500 Hz, the energy level of the spurious directions vary between 0 and 10 dB below the reference level. This means that if the bandwidth signal is less than 2500 Hz, the method cannot separate

erroneous directions from the correct direction. For b_d larger than 4500 Hz, the levels are 20 dB lower than the reference level. The first erroneous value is much smaller than the reference value. This means that, for this mesh, if the bandwidth of the signal is larger than 4500 Hz, the method will provide satisfying results.

5.3. Correlated sources

As said in the introduction, in many applications, our interest is to use ISIT to determine the directions of the main reflections on the walls of a hall. The reflected sound fields are emitted by the images of the real source. The images are obviously correlated with the source itself. The point here is to examine how ISIT can be applied to correlated sources.

In the simple case of two correlated point sources 1 and 2 in a free-field, it is possible to obtain an analytical expression of the cross-correlation function. $C_{x_n,x_m}(\tau)$ has four peaks. Two of them correspond to source 1 and source 2, respectively. The other two are "cross-peaks" which appear because of interactions between sources 1 and 2. These cross-peaks can lead to the identification of two wrong directions. They correspond to two delays τ_{12}^{nm} and τ_{21}^{nm} but do not correspond to real sources. However, it is possible to determine geometrical conditions (on the respective distances between the sources and between the microphones) so that the two peaks do not appear in the integration intervals $[-\mathbf{r}_{nm}/c; +\mathbf{r}_{nm}/c]$. In the applications described here (halls of large dimensions), these conditions are generally satisfied, except for a small number of pairs of microphones. In this case, the algorithm is quite robust and ISIT do not identify erroneous directions. Also numerical tests have shown that, in rectangular halls of large dimensions, the cross-peaks generally have small amplitudes and therefore have a weak effect on the results. Another important point is that, in practical situations, sound fields radiated by a machine in different directions are generally only partly correlated and this reduces the risk of erroneous directions. From all these considerations, it was assumed that ISIT could be applied in the case of correlated sources. The examples presented in the next section show that the results obtained are quite satisfactory.

6. Experimental tests

Several experimental tests were run to check the validity of the method. Two examples are reported here. The first example is the case of a point source in a semi-anechoic room. A panel of finite dimension had been installed close to the source. In this case, the sound field measured on the array is approximated as the sum of the direct field and the field emitted by three image sources. This may be seen as a problem with four correlated sources. The second example is the case of respectively one and two sources located in a reverberant rectangular room. In both examples, the sound field emitted by the sources has a broad-band spectrum.

For the measurements, Bruël and Kjaer, 1/2 inch, microphones were used for the array and the signals were processed through an OROS OR25 data system. The signals duration was 30 s. The sampling frequency was $F_e = 25.6$ kHz. The first step consists in computing the cross-spectral densities by using a classical periodogram technique with 46 blocks of 16 384 points. The cross-correlation functions are obtained as the inverse Fourier transform of the cross-spectral densities. They are computed by using the PhaT transform (Phase transform).

The ISIT method is based on the measurements of the time delays between all the sensors or equivalently of the phases of the cross-spectral densities. Some extra phase differences are introduced in the measurements because of the equipment itself (microphones, data system, cables, etc.). These differences can be measured with an intensity calibrator. In the examples presented here, they were smaller than 0.6° at 5 kHz. Therefore they had a negligible effect on the accuracy of the results.

6.1. Source in a semi-anechoic room

In this example, a broad-band point source is located in a semi-anechoic room at 1.6 m above the ground. The emitted signal is a pink noise. A panel of finite dimension ($1.25 \times 2\,\mathrm{m}^2$) is situated at a distance of 1 m from the array. It is made of plywood covered with thin perforated plates.

With this geometry, there are four main sources or paths to consider (see Fig. 9):

- direct path, which corresponds to the direction $\phi = 105^\circ$, $\theta = 85^\circ$,
- reflection on the ground, $\phi = 105^\circ$, $\theta = 135^\circ$,
- reflection on the panel, $\phi = 52^\circ$, $\theta = 86^\circ$,
- ground-panel double reflection, $\phi = 52^\circ$, $\theta = 128^\circ$.

Fig. 10 shows an angular map of the values of the coefficients $(E_l), l = 1, \ldots, K$ obtained from ISIT. Each value corresponds to a cell Ω_l as defined in Fig. 2 and therefore to a direction (ϕ_l, θ_l). The horizontal and the vertical scales correspond respectively to the angle ϕ varying between 0° and 360° and to the angle θ varying between 0° and 180°. The angular width of the cells is 10°. The values of E_l are presented on a logarithmic scale. The levels are all normalized to the largest value of the coefficients E_l which is chosen as the reference value. This means that the maximum level of 0 dB corresponds to this largest value. Four sources, corresponding to the real source and three image sources, are identified quite accurately, with their relative amplitudes. It can be seen that the highest energy cell (number 1) corresponds to the real source. The panel-reflection (number 2) corresponds to a higher level than the ground-reflection (number 3). This was expected since the panel is closer to the source and is more reflecting, in this experiment, than the floor of the semi-anechoic room which is covered with a layer of linoleum. Cell number 4 corresponds to the double reflection on the floor and on the panel.

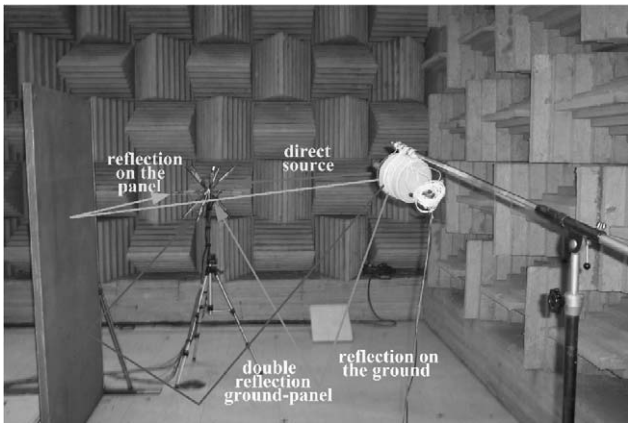

Fig. 9. View of the experiment in the semi-anechoic room.

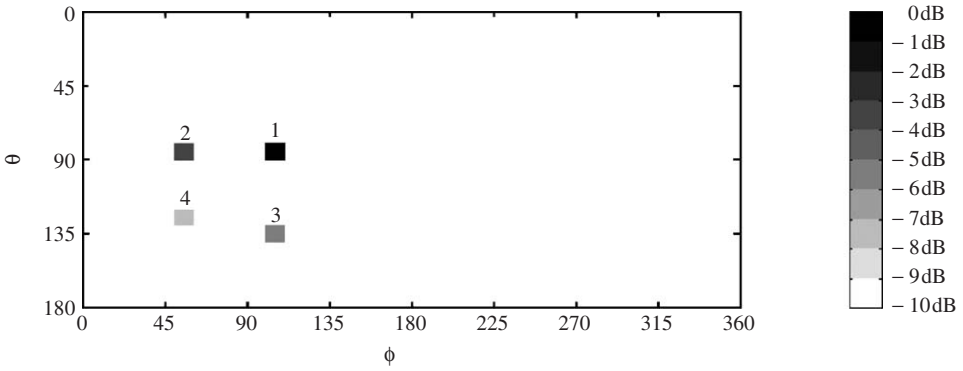

Fig. 10. Angular map of energy levels. Four sources in the semi-anechoic room.

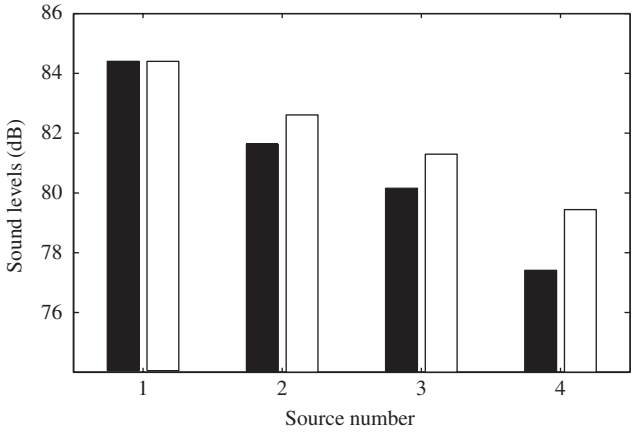

Fig. 11. Sound levels emitted by the four sources and received on the array. ISIT method (black bars); image method (white bars). Levels in dB (ref. 2×10^{-5} Pa).

In order to show the efficiency of the method, a comparison of the sound levels emitted by the four sources and received on the array is presented in Fig. 11. The black bars correspond to the values of the levels deduced from ISIT. The white bars correspond to the values computed directly by an image method. The input data of the image method are the geometrical data, the amplitude of the source and the reflection coefficients of the panel and the floor. The amplitudes of the real source and of the first two images are obtained with an accuracy of 1 dB; the accuracy is of 2 dB for the amplitude of the third image.

Let us also add that, for all the tests conducted in the semi-anechoic room, the ratio between the real directions of energy and the wrong directions is larger than 25 dB.

In this example, the results of the ISIT method have also been used to evaluate the energy absorption coefficients of the floor and the panel. In the case of the floor, for instance, it is assumed that the energy of the cell corresponding to the floor-reflection is proportional to the energy of the real source reflected by the floor divided by the square distance between the ground image source and the center of the array. Here, the angle of incidence of the ground-reflected ray is equal to 45°. The corresponding absorption coefficient deduced from ISIT method is equal to 0.19. The value of the absorption coefficient of the floor has also been measured by a two-microphone technique [32]. The average value, obtained over the frequency range 125–4000 Hz, for an angle of incidence of 45°, is 0.17 which is quite close to the value obtained with ISIT. This shows that the ISIT method could also provide an interesting way to determine absorption coefficients of finite-dimension panels.

6.2. *Sources in a reverberant rectangular room*

In this second example, two uncorrelated broad-band sources are located in a rectangular empty room. The dimensions of the room are $29.63 \times 7.7 \times 3.68\,\mathrm{m}^3$. A 3D-scheme of the geometry is presented in Fig. 12.

The four lateral walls are named wall1, wall2, wall3 and wall4. They are made of plastered bricks. The room has a concrete floor and an absorbing ceiling. The reverberation time measured at 1000 Hz octave is equal to 2 s. This corresponds to a rather reverberant room. Three cases were studied:

- the sound field is emitted by a Pioneer TSE1077 loudspeaker (source 1) located at a point $S1 = (3.63, 3.35, 0.05)$,
- the sound field is emitted by a pressure driver (source 2) located at a point $S2 = (6.35, 17.63, 0.05)$,
- the sound field is emitted by sources 1 and 2 together.

The center of the array is located at $M = (4.35, 11.63, 1.6)$. All units are in meters. The positions of source 1 and source 2 respectively correspond to the directions $(\phi_1 = 262.9°, \theta_1 = 100.9°)$ and $(\phi_2 = 71.6°, \theta_2 = 103.8°)$.

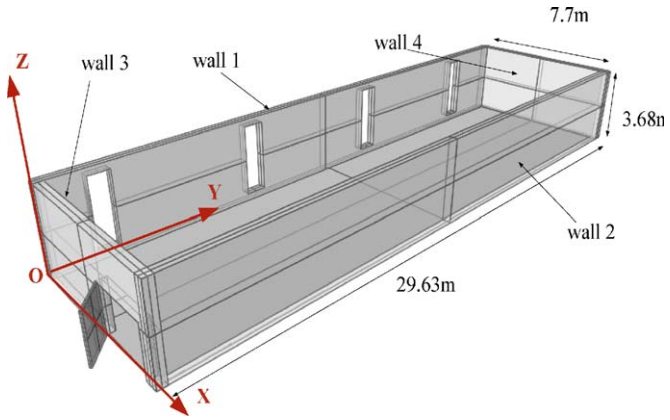

Fig. 12. Geometry of the reverberant hall.

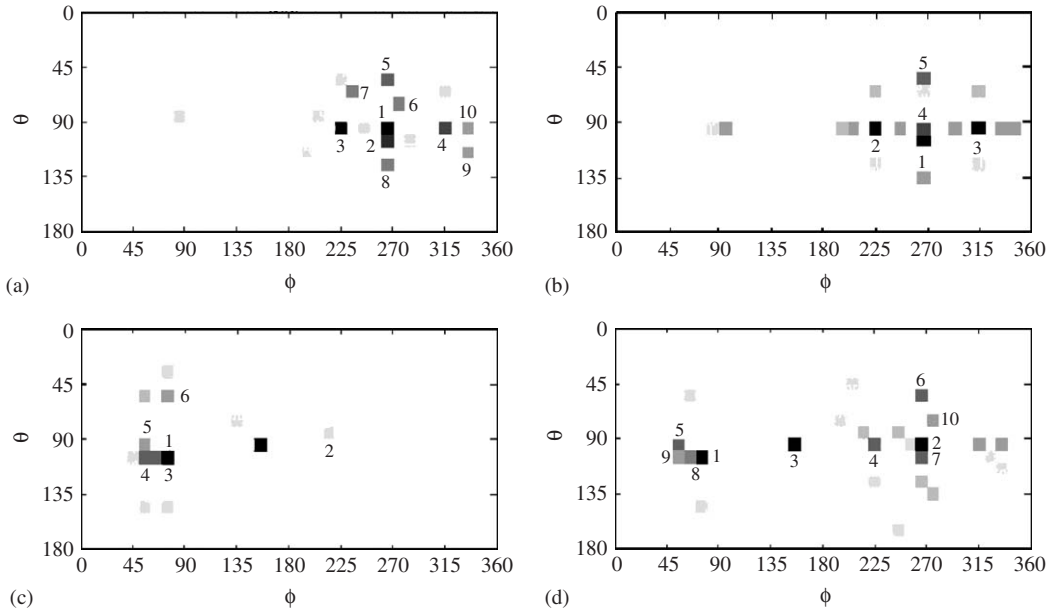

Fig. 13. Angular maps of energy levels. Sources in the reverberant rectangular hall. (a) ISIT map for source 1; (b) theoretical map for source 1; (c) ISIT map for source 2; (d) ISIT for sources 1 and 2. Same scale as in Fig. 10.

Fig. 13 presents the angular maps obtained for the three cases with ISIT. The numbers written next to the cells correspond to decreasing orders of amplitude. In addition, in the case of source 1 alone, the theoretical map (b) presents the sound levels computed directly by an image method. The aim was to compare the main directions of energy obtained with both methods and not the exact values of the amplitudes. Indeed, it is not possible to characterize the walls by some accurate values of reflection coefficients because they do not have homogeneous properties, from both a geometrical and an acoustic point of view. Thus the walls were simply characterized by constant reflection coefficients averaged over the whole frequency range. In this case, the image method provides correct information on the directions of arrival but not on the amplitudes. The directions of arrival presented on the experimental map (a) and the theoretical map (b) are quite similar. The position of the source itself corresponds to cell number 2. Cell 1 is associated with the reflection on wall3. Actually, cells 1 and 2 correspond to very close directions. Cells 3 and 4 correspond to reflections on wall1 and wall2 respectively. Cell 5 corresponds to a reflection on the ceiling.

In the case of source 2 alone (c), cell 1 corresponds to the direct path. Cells 2 and 5 correspond to reflections on wall1 and wall2 respectively. Cells 3 and 4 correspond to ground reflections close to the source. Cell 6 corresponds to a reflection on the ceiling.

When both sources are used (d), the main directions of arrival are again well determined. The hierarchy of the directions obtained for each source alone is globally found as expected, except for one or two reflections. This could be explained by some interference phenomena between the two sources and their reflections.

In all the angular maps presented here, the scale of the normalized levels extends from 0 to −10 dB. Let us recall that in the industrial applications of ISIT, the interest is to determine the sources or areas that must be treated in order to reduce the noise levels at given places. We have therefore chosen to use the maps as follows: The directions of energy are gathered into several sets. The first set includes the directions with amplitudes between 0 and −3 dB, it corresponds to the sources and areas that must be treated first. The second set includes the directions with amplitudes between −3 and −6 dB, and so on. This means that the method does not need to be highly accurate in the evaluation of the amplitudes.

These examples show that ISIT method is an efficient tool for the kind of applications we are interested in. A MUSIC algorithm associated with a coherent focusing method has also been applied to this configuration. The positions of the main directions as well as their amplitudes are not determined properly. This could be explained partly by the fact that MUSIC is not suited to the cases of reverberant halls where too large a number of sources (or reflections) has to be determined.

Next section describes the results obtained in a more realistic case.

7. Case of a surface-planing machine in a factory hall

This example corresponds to the case of a planing machine in a very cluttered hall (see Fig. 14). The dimensions of the hall are $26 \times 11 \times 8.3\,m^3$ (see Fig. 15). Its reverberation time in the 1000 Hz octave band is equal to 2.8 s. With respect to its volume, the hall can be considered as semi-reverberant or reverberant.

Fig. 16 shows the position of the machine and the position of the center of the array.

When operated, the planing machine generates several noise sources due to the tool itself (a chisel), the electric engine, the vibrations of the structure, etc. In the present case, the noise of the tool however is the main source. The position of the tool on the machine corresponds to the direction ($\phi_t = 110°$, $\theta_t = 95°$).

Fig. 17 presents, as a function of frequency, the sound pressure level measured at one point located 9.6 m from the machine (Ref. 2×10^{-5} Pa). The three top curves represent the sound spectrum of the machine (with an octave band, 3rd-octave band and narrow-band analysis). The bottom curve presents the spectrum of the background noise measured in the hall. It can be seen that the spectrum of the machine is made of a combination of a broad-band spectrum and a harmonic complex sound generated by the electric engine, the tool itself, etc. Despite these emerging frequencies, ISIT can be used.

Fig. 18 presents the angular map obtained with ISIT. Cell 1 corresponds to the position of the chisel. Cells 1 and 4 correspond to close directions which are related to the position of the machine and to a first reflection on wall4. Cells 2 and 6 are related to reflections on wall2, cells 3 and 5 to reflections on wall1. The ceiling does not provide so much energy, only cell 9 corresponds to reflections on this surface.

Fig. 14. Views of the planing machine and of the industrial hall.

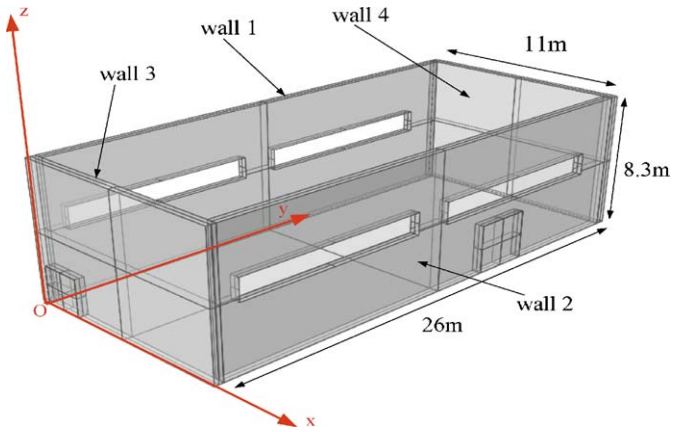

Fig. 15. Geometry of the industrial hall.

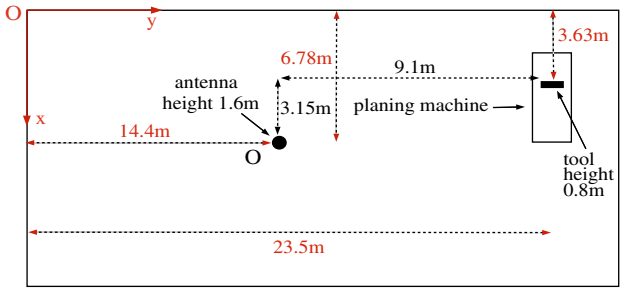

Fig. 16. Top view of the experiment in the industrial hall.

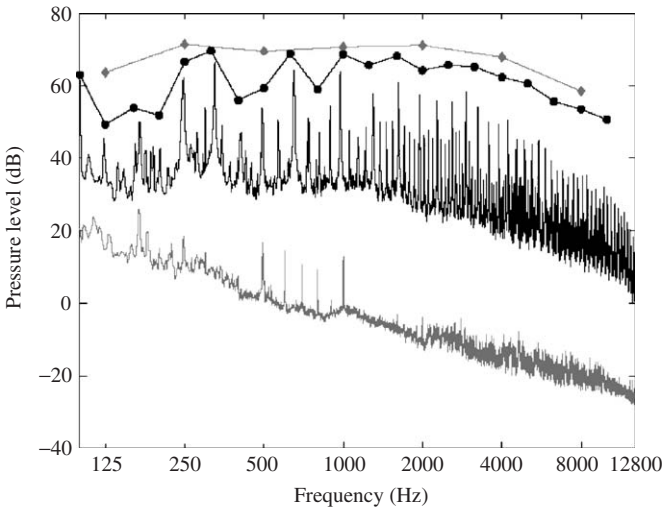

Fig. 17. Sound levels in dB (ref. 2×10^{-5} Pa). The three top curves: sound spectrum of the machine (octave band, 3rd-octave band and narrow-band). Bottom curve: spectrum of the background noise measured in the industrial hall.

More detailed information may be deduced from this map by looking more closely to the geometry of the hall. It can be seen for instance that cells 2 and 6 are located close to a highly reflecting steel door (wall2) and to a window. Cells 5 and 9 correspond to an aluminum panel located above a window on wall1. Cell 3 is close to a closet with a glass-door. The cells revealed by ISIT do correspond to highly reflecting areas of the hall.

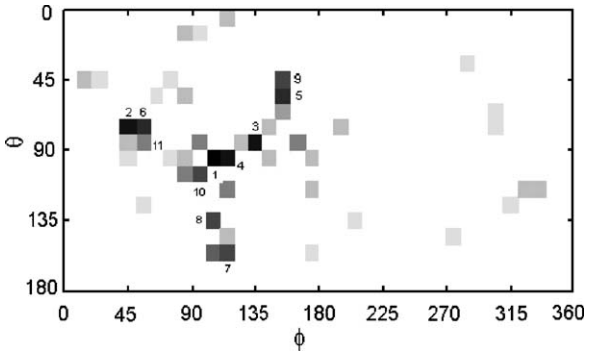

Fig. 18. Angular map of energy levels in the industrial hall. Same scale as in Fig. 10.

8. Conclusion

The examples developed here show that ISIT is a promising tool to determine the sources or areas that provide the main contributions to the noise levels measured at a given place. It was specially developed to fulfill the specific constraints in industrial halls: The array must have small dimensions and a small number of receivers, the machines operates 24 h a day and cannot be turned off and on, the halls are generally quite reverberant.

All the results presented here were obtained from measured data. The first one in the semi-anechoic room shows that the method can provide accurate results with correlated sources. The second one with two uncorrelated sources in the empty hall shows that the method can determine a large number of reflections. The third one obtained with the planing machine shows that ISIT still provides satisfactory results in conditions very similar to realistic situations.

However, this method can still be improved. Three of the next steps will be to reduce the computing time of the matrix deduced from the cross-correlation of the signals, to apply the method to more complicated cases such as a reverberant hall with several machines, and to extend the method to narrow-band spectra.

Finally, from a theoretical point of view, it would be interesting to compare in more details the different aspects of methods such as ISIT developed in the time domain and MUSIC developed in the frequency domain. Obviously, these methods correspond to two different descriptions of the same kind of problem. Examining and comparing their theoretical developments in detail will provide a better understanding of their respective advantages and domains of application.

Appendix A. Computation of coefficients of matrices B(n, m)

The cross-spectral density $S_{x_n,x_m}(v)$ of two signals $x_n(t)$ and $x_m(t)$ is given by

$$S_{x_n,x_m}(v) = \int_{\Omega} \alpha(\phi,\theta) \exp\left(-2\mathrm{i}\pi v \frac{\mathbf{n}(\phi,\theta).\mathbf{r}_{nm}}{c}\right) \sin\theta \,\mathrm{d}\theta \,\mathrm{d}\phi. \tag{A.1}$$

This can be written as a sum of spherical harmonics, by using the following series for the exponential term [33–35]:

$$\exp(-\mathrm{i}k\mathbf{n}(\phi,\theta).\mathbf{r}_{nm}) = 4\pi \sum_{p=0}^{p=+\infty} (-\mathrm{i})^p j_p(kd_{nm}) \sum_{q=-p}^{q=p} Y_{pq}(\theta_c,\phi_c) Y^*_{pq}(\theta,\phi), \tag{A.2}$$

where $k = \dfrac{2\pi v}{c}$. $Y_{pq}(\theta,\phi)$ is a spherical harmonic function defined by [36]:

$$Y_{pq}(\theta,\phi) = \sqrt{\frac{2p+1}{4\pi}\frac{(p-|q|)!}{(p+|q|)!}} P_p^{|q|}(\cos\theta) \mathrm{e}^{\mathrm{i}q\phi}, \tag{A.3}$$

where P_p^q is the Legendre function of degree p and order q. j_p is the spherical Bessel function of the first kind [36].

By inverting sum and integral, the cross-spectral density can be written as

$$S_{x_n,x_m}(v) = 4\pi \sum_{p=0}^{p=+\infty} (-\mathrm{i})^p j_p(kd_{nm}) \sum_{q=-p}^{q=p} \int_\Omega Y_{pq}(\theta_c,\phi_c)\alpha(\phi,\theta) Y_{pq}^*(\theta,\phi) \sin\theta \,\mathrm{d}\theta \,\mathrm{d}\phi. \tag{A.4}$$

If $\alpha(\phi,\theta)$ is assumed to be constant on each Ω_l, it becomes

$$S_{x_n,x_m}(v) = 4\pi \sum_{l=1}^{l=K} \alpha_l \sum_{p=0}^{p=+\infty} (-\mathrm{i})^p j_p(kd_{nm}) \sum_{q=-p}^{q=p} \int_{\Omega_l} Y_{pq}(\theta_c,\phi_c) Y_{pq}^*(\theta,\phi) \sin\theta \,\mathrm{d}\theta \,\mathrm{d}\phi. \tag{A.5}$$

Spherical harmonics Y_{pq} are replaced by their expression (A.3) and α_l by $E_l/\Delta\Omega_l$. The cell Ω_l is assumed to be bounded in ϕ by the angles ϕ_1^l and ϕ_2^l and in θ by θ_1^l and θ_2^l. This leads to

$$\begin{aligned} S_{x_n,x_m}(v) = & \sum_{l=1}^{l=K} \frac{E_l}{\Delta\Omega_l} \sum_{p=0}^{p=+\infty} (-\mathrm{i})^p j_p(kd_{nm}) \\ & \times \sum_{q=-p}^{q=p} \int_{\phi_1^l}^{\phi_2^l} \int_{\theta_1^l}^{\theta_2^l} (2p+1) \frac{(p-|q|)!}{(p+|q|)!} P_p^{|q|}(\cos\theta_c) \\ & \times P_p^{|q|}(\cos\theta) \mathrm{e}^{-\mathrm{i}q(\phi-\phi_c)} \sin\theta \,\mathrm{d}\theta \,\mathrm{d}\phi. \end{aligned} \tag{A.6}$$

The integral with respect to ϕ is obtained analytically, and finally

$$S_{x_n,x_m}(v) = \sum_{l=1}^{l=K} \frac{E_l}{\Delta\Omega_l} \sum_{p=0}^{p=+\infty} (-\mathrm{i})^p \gamma_p^l j_p(kd_{nm}), \tag{A.7}$$

where γ_p^l is equal to

$$\begin{aligned} \gamma_p^l = (2p+1) \Bigg[& \Delta\phi P_p(\cos\theta_c) \int_{\theta_1^l}^{\theta_2^l} P_p(\cos\theta) \sin\theta \,\mathrm{d}\theta \\ & + 2 \sum_{q=1}^{q=p} \frac{(p-q)!}{(p+q)!} \frac{\sin(q(\phi_2^l-\phi_c)) - \sin(q(\phi_1^l-\phi_c))}{q} \\ & \times P_p^q(\cos\theta_c) \int_{\theta_1^l}^{\theta_2^l} P_p^q(\cos\theta) \sin\theta \,\mathrm{d}\theta \Bigg]. \end{aligned} \tag{A.8}$$

The cross-correlation function $C_{x_n,x_m}(\tau)$ is obtained as the inverse Fourier transform of the cross-spectral density. In formula (A.7), $j_p(kd_{nm})$ is the only term which depends on frequency (because k depends on v). The inverse Fourier transform of $j_p(kd_{nm})$ can be written as

$$TF^{-1}[j_p(kd_{nm})] = \frac{1}{2\pi} \int_\infty^\infty j_p\left(\frac{\omega}{c} d_{nm}\right) \mathrm{e}^{\mathrm{i}\omega\tau} \,\mathrm{d}\omega \tag{A.9}$$

or

$$TF^{-1}[j_p(kd_{nm})] = \frac{c}{2d_{nm}} \frac{1}{\sqrt{2\pi}} \int_{-\infty}^\infty \frac{J_{p+\frac{1}{2}}(\omega)}{\sqrt{\omega}} \mathrm{e}^{\mathrm{i}\omega\frac{c}{d_{nm}}\tau} \,\mathrm{d}\omega, \tag{A.10}$$

where $\omega = 2\pi v$. J_p is the Bessel function of order p. The following relation [36]:

$$\int_{-\infty}^\infty \frac{J_{p+\frac{1}{2}}(\omega)}{\sqrt{\omega}} \mathrm{e}^{-\mathrm{i}\omega t} \,\mathrm{d}\omega = \begin{cases} (-\mathrm{i})^p \sqrt{2\pi} P_p(t) & \text{if } t^2 \leqslant 1, \\ 0 & \text{if } t^2 > 1 \end{cases} \tag{A.11}$$

is used in formula (A.10). This gives

$$TF^{-1}[j_p(kd_{nm})] = \begin{cases} \dfrac{c}{2d_{nm}}(-\mathrm{i})^p P_p\left(-\dfrac{c}{d_{nm}}\tau\right) & \text{if } -\dfrac{d_{nm}}{c} \leqslant \tau \leqslant \dfrac{d_{nm}}{c}, \\ 0 & \text{if not.} \end{cases} \tag{A.12}$$

From Eqs. (A.7) and A.12, $C_{x_n x_m}(\tau)$ is expressed for all τ in $[-\frac{d_{nm}}{c}; \frac{d_{nm}}{c}]$ as

$$C_{x_n,x_m}(\tau) = \sum_{l=1}^{l=K} \frac{E_l}{\Delta\Omega_l} \frac{c}{2d_{nm}} \sum_{p=0}^{p=+\infty} (-1)^p \gamma_p^l P_p\left(-\frac{c}{d_{nm}}\tau\right). \tag{A.13}$$

After integration with respect to τ on $I_{nm}^i = [\tau_{\min}^i(n,m); \tau_{\max}^i(n,m)]$, we obtain for all $i = 1, \ldots, K$:

$$C^i(n,m) = \sum_{l=1}^{l=K} E_l \frac{1}{\Delta\Omega_l} \sum_{p=0}^{p=+\infty} \frac{(-1)^p}{2} \gamma_p^l \int_{A_{nm}^i} P_p(\tau)\,\mathrm{d}\tau, \tag{A.14}$$

where

$$A_{nm}^i = \left[-\frac{c}{d_{nm}}\tau_{\max}^i(n,m); -\frac{c}{d_{nm}}\tau_{\min}^i(n,m)\right]. \tag{A.15}$$

Comparing Eqs. (12) and (A.14) gives

$$\beta_l^i(n,m) = \frac{1}{\Delta\Omega_l} \sum_{p=0}^{p=+\infty} \frac{(-1)^p}{2} \gamma_p^l \int_{A_{nm}^i} P_p(\tau)\,\mathrm{d}\tau. \tag{A.16}$$

References

[1] M. Sidki, Mesure de l'intensité acoustique, application à la localisation et la caractérisation des sources, PhD Thesis, Université Paul Sabatier Toulouse III, 1985.

[2] M. Besombes, Modélisation de sources de bruit industrielles par identification paramétrique à partir de mesures d'intensité acoustique, PhD Thesis, Université Paul Sabatier Toulouse III, 1989.

[3] F. Tolstoy, *Matched Field Processing for Underwater Acoustics*, World Scientific, New York, 1993.

[4] J. Capon, High resolution frequency wavenumber spectrum analysis, *Proceedings of the IEEE* 57 (8) (1969) 1408–1418.

[5] G. Bienvenu, L. Kopp, Méthodes haute résolution pour la localisation de sources rayonnantes, *L'onde électrique* 64 (2) (1984) 28–37.

[6] H. Schmidt, Environmentally tolerant beamforming for high resolution matched filed processing: deterministic mismatch, *Journal of the Acoustical Society of America* 88 (4) (1990) 1851–1862.

[7] I. Ziskind, M. Wax, Maximum likelihood localization of multiple sources by alternating projection, *IEEE Transactions on Acoustics, Speech and Signal Processing* 36 (10) (1988) 1553–1560.

[8] P. Stoica, A. Nehoral, Music, maximum likelihood, and Cramer–Rao bound, *IEEE Transactions on Acoustics, Speech and Signal Processing* 37 (5) (1989) 720–741.

[9] J. Benesty, Adaptive eigenvalue decomposition algorithm for passive acoustic source localization, *Journal of the Acoustical Society of America* 107 (1) (2000) 384–391.

[10] J.C. Preisig, Robust maximum energy adaptive matched field processing, *IEEE Transactions on Signal Processing* 42 (7) (1994) 1585–1593.

[11] H. Cox, R.M. Zeskind, M.M. Owen, Robust adaptive beamforming, *IEEE Transactions on Acoustics, Speech and Signal Processing* 35 (10) (1987) 1365–1376.

[12] S.U. Pillai, B. Ho-Kwon, Forward/backward spatial smoothing techniques for coherent signal identification, *IEEE Transactions on Acoustics, Speech and Signal Processing* 37 (1) (1989) 8–14.

[13] Y.-M. Chen, On spatial smoothing for two dimensional direction of arrival estimation of coherent signals, *IEEE Transactions on Signal Processing* 45 (7) (1997) 1689–1696.

[14] D.N. Swinger, J. Krolik, Source location bias in the coherently focused high resolution broadband beamformer, *IEEE Transactions on Acoustics, Speech and Signal Processing* 37 (1) (1989) 143–145.

[15] P. Stoica, B. Ottersten, M. Viberg, R.L. Moses, Maximum likelihood array processing for stochastic coherent sources, *IEEE Transactions on Signal Processing* 44 (1) (1996) 96–105.

[16] H. Hung, M. Kaveh, Focusing matrices for coherent signal processing, *IEEE Transactions on Acoustics, Speech and Signal Processing* 36 (8) (1988) 1272–1281.

[17] H. Wang, M. Kaveh, Coherent signal subspace processing for detection and estimation of angles of arrival of multiple wideband sources, *IEEE Transactions on Acoustics, Speech and Signal Processing* 33 (4) (1985) 823–831.
[18] S. Bourennane, Traitement d'antenne à large bande de fréquence, PhD Thesis, Institut National Polytechnique de Grenoble, 1990.
[19] T.-J. Shan, M. Wax, T. Kailath, On spatial smoothing for direction-of-arrival estimation of coherent signals, *IEEE Transactions on Acoustics, Speech and Signal Processing* 33 (4) (1985) 806–811.
[20] Y. Yamaski, T. Itow, Measurement of spatial information in sound fields by closely located four point microphone method, *Journal of Acoustical Society of Japan* 10 (2) (1989) 101–110.
[21] K. Sekiguchi, S. Kimura, T. Hanyuu, Analysis of sound field on spatial information using a four-channel microphone system based on regular tetrahedron peak point method, *Applied Acoustics* 37 (1986) 305–323.
[22] A. Abdou, R.W. Guy, Spatial informations of sound fields for room-acoustics evaluation and diagnosis, *Journal of the Acoustical Society of America* 100 (5) (1996) 3215–3225.
[23] B.N. Gover, J.G. Ryan, M.R. Stinson, Microphone array measurement system for analysis of directional and spatial variations of sound fields, *Journal of the Acoustical Society of America* 112 (5) (Part 1) (2002) 1980–1991.
[24] M. Brandstein, D. Ward, *Microphone Arrays—Signal Processing Techniques and Applications*, Springer, Berlin, 2001.
[25] M.S. Brandstein, A Framework for Speech Source Localisation using Sensor Arrays, PhD Thesis, Division of Engineering at Brown University, 1995.
[26] S.M. Baxter, C.L. Morfey, *Angular Distribution—Analysis in Acoustics*, Springer, Berlin, 1986.
[27] W.K. Blake, R.V. Waterhouse, The use of cross-spectral density measurements in partially reverberant sound fields, *Journal of Sound and Vibration* 54 (4) (1977) 589–599.
[28] B. Rafaely, Spatial-temporal correlation of a diffuse sound field, *Journal of the Acoustical Society of America* 107 (6) (2000) 3254–3258.
[29] C.L. Lawson, R.J. Hanson, *Solving Least Squares Problems*, Prentice-Hall, Englewood Cliffs, NJ, 1974.
[30] B. Rafaely, Plane-wave decomposition of the sound field on a sphere by spherical convolution, *Journal of the Acoustical Society of America* 116 (4) (Part 1) (2004) 2149–2157.
[31] C. Knapp, G.C. Carter, The generalized correlation method for estimation of phase delay, *IEEE Transactions on Acoustics, Speech and Signal Processing* 24 (4) (1976) 320–326.
[32] J.F. Allard, B. Sieben, Measurement of acoustic impedance in a free field with two microphones and spectrum analyser, *Journal of the Acoustical Society of America* 77 (4) (1985) 1617–1618.
[33] P.M. Morse, H. Feshbach, *Methods of Theoretical Physics—part I and II*, McGraw-Hill Book Company, New York, 1953.
[34] P.D. Teal, T.D. Abhayapala, R.A. Kennedy, Spatial correlation for general distributions of scatterers, *ICASSP'02*, 2002, pp. 2833–2836.
[35] P.M. Morse, K.U. Ingard, *Theoretical Acoustics*, McGraw-Hill Book Company, New York, 1968.
[36] M. Abramowitz, I. Stegun, *Handbook of Mathematical Functions*, Dover Publication, New York, 1972.